Infiltration and Wetting of Alumina Particulate Preforms by Aluminum and Aluminum-Magnesium Alloys

TAMALA R. JONAS, JAMES A. CORNIE, and KENNETH C. RUSSELL

The infiltration and wetting of alumina particulates by Al and by Al-Mg alloys was studied through pressure infiltration experiments. In these experiments, a noninvasive capacitance technique was used to determine the infiltration front position as a function of time. An unsaturated slug flow model was used to interpret the infiltration results and determine capillary pressures characteristic of the infiltration process. The characteristic capillary pressures for Al, Al-2Mg, and Al-3Mg at 750 °C and Al-2Mg at 850 °C were not significantly different. Therefore, contrary to usual belief, Mg did not significantly aid the pressure infiltration process. At 750 °C, the maximum values of the contact angle calculated from these capillary pressures were 106 deg for Al and 105 deg for Al-2Mg and Al-3Mg. These contact angle values indicate substantial removal of the oxide layer on the surface of the liquid metal during the infiltration process. The small difference in the contact angles indicates that magnesium had little effect on the wetting of alumina by aluminum. The small effect of Mg on the wetting may be due to absence of reactive wetting at the infiltration speeds present in the experiments and to partial disruption of the oxide layer on the surface of the liquid metal during the infiltration process.

I. INTRODUCTION

THE pressure infiltration process for making metal matrix composites uses an applied pressure difference to force liquid metal into a preform of reinforcement material. The pressure required for a given degree of infiltration is expected to depend in part on the extent to which the liquid metal wets the preform material. One approach to reducing the pressures required in the process, thus making it more economical, is to consider using alloys that better wet the preform material.

The details of the infiltration process affect the relationship between the applied pressure difference and the wetting. The pressure difference across the liquid-vapor interface in a pore is known as the capillary pressure. Unless vacuum is present in the preform, liquid metal will displace gas from the preform during the infiltration process. If this gas is not trapped in the preform, then an increase in the applied pressure difference will increase the capillary pressure and fill more of the pore space with fluid. In this case, the capillary pressure or applied pressure difference required for a given degree of infiltration can be related to the changes in interfacial energy occurring during infiltration and thus to more standard measures of wetting.

In this work, the infiltration and wetting of alumina particulates by Al and Al-Mg alloys was investigated. Al-Mg alloys were selected because Mg has been observed to improve the wetting between liquid aluminum and alumina in sessile-drop experiments, in some stirring processes, and in the LANXIDE* process.[1-4] The infiltration was studied by tracking the position of the infiltration front as a function of time with a capacitance technique. A fluid flow model was used to interpret these results and determine capillary pressures characteristic of the infiltration process. Contact angles were obtained from the characteristic capillary pressures using a thermodynamic energy balance both with and without terms correcting for irreversibility and incomplete filling of the pore space. Although determination of the wetting from the capillary pressure is less direct than conventional measurement methods, it provides information about the wetting under actual process conditions. These conditions typically differ from those present in conventional sessile-drop wetting experiments because the solid surfaces are rough and because the liquid metal is flowing, rather than stationary, which could disturb its surface oxide layer and limit the effect of reaction.

*LANXIDE is a trademark of LANXIDE Corp., Newark, DE.

TAMALA R. JONAS, Research Engineer, is with American National Can Beverage Technical Center, Elk Grove Village, IL 60007. JAMES A. CORNIE, Visiting Scientist, Department of Mechanical Engineering, and KENNETH C. RUSSELL, Professor, Department of Materials Science and Engineering and Department of Nuclear Engineering, are with Massachusetts Institute of Technology, Cambridge, MA 02139.

Manuscript submitted July 18, 1994.

II. THEORY

A. *Unsaturated Slug Flow Infiltration Model*

The saturation profile across the infiltrated region determines the appropriate infiltration model. The saturation, S, is defined as the fraction of pore space infiltrated. The porosity profile in the solidified composite was assumed to indicate the saturation profile during infiltration. In the solidified composite, the average porosity was approximately uniform away from the infiltration front. Near the infiltration front, the porosity increased. Since some porosity was found even near the preform entrance, it is possible that the preform was not completely infiltrated.

This section derives an infiltration model for the idealized case where the saturation level of the infiltrated region is uniform up to the infiltration front, which approximately corresponds to the porosity profile in the samples after solidification. This saturation profile is describable by a slug flow model. Since some porosity was

found in the infiltrated samples, the model allows the saturation in the infiltrated region to be less than one. Figure 1 illustrates an idealized saturation profile and a corresponding saturation *vs* capillary pressure curve for the unsaturated slug flow model. In this figure, S_u denotes the uniform saturation level, L is the total infiltration length, and ΔP_c is the capillary pressure.

The infiltration model gives the position of the infiltration front as a function of time through relating the flow rate predicted by Darcy's law for unidirectional flow to the advance rate of the front. Darcy's law[5] may be written as

$$q = -\frac{k(S)\, dP}{\mu\, dx} \qquad [1]$$

where q is the volumetric flow rate per unit cross-sectional area, $k(S)$ is the permeability, μ is the liquid viscosity, and dP/dx is the local pressure drop. In the region where the saturation is constant, q, μ, and $k(S)$ will not vary with position. This means the local pressure drop dP/dx will also be constant and equal to the pressure drop across the region divided by the length of the region, L. Therefore,

$$q = \frac{k(S_u)\,[\Delta P_{tot} - \Delta P_c(S_u)]}{\mu L} \qquad [2]$$

In this equation, ΔP_{tot} is the total applied pressure difference and ΔP_c is the capillary pressure, which is expected to depend on the saturation. Since the saturation is zero ahead of the infiltration front,

$$q = S_u \phi \frac{dL}{dt} \qquad [3]$$

where ϕ is the preform porosity. For a constant applied pressure difference, Eqs. [2] and [3] can be combined and integrated to yield

$$\frac{L^2}{t} = \frac{2k(S_u)\,[\Delta P_{tot} - \Delta P_c(S_u)]}{\mu S_u \phi} \qquad [4]$$

If the pressure difference driving the flow becomes constant only after some time, it will be $\partial L^2/\partial t$, which is equal to the right-hand side of Eq. [4]. For this case, it is possible to obtain an averaged estimate of $\Delta P_c(S_u)$ by plotting $\partial L^2/\partial t$ *vs* ΔP_{tot} for experiments conducted at different pressures. $\Delta P_c(S_u)$ will be the pressure axis intercept of the straight line through the data points. Equation [4] will predict the same results as the equation for saturated slug flow if the ratio $k(S_u)/S_u$ is equal to the saturated permeability.

Because the saturation gradient observed experimentally in the tip region near the infiltration front was not a step function, as shown in Figure 1, some approximations are involved in applying the model to the experiments. The approximations involved in applying Eqs. [2] and [3] are relatively small since the tip region where the gradient occurred was usually small in comparison to the total length. However, the more gradual change in saturation level with distance implies a more gradual change in saturation level with capillary pressure, since the capillary pressure is a function of distance in the sample. Therefore, the characteristic capillary pressure at which changes in saturation become indistinguishable will not be as sharply defined with respect to the saturation *vs* capillary pressure curve as in the ideal case. For better comparison of the characteristic capillary pressures of different alloys, the pressures should occur at a similar saturation.

B. *Conversion between Capillary Pressures and Contact Angles*

If the filling process is complete and reversible, then the pressure-volume work required to fill the preform will be equal to the change in surface energy involved in converting all of the solid-vapor interface to solid-liquid interface.[6,7,8] The energy balance for these conditions can be written as follows:

$$\cos\theta = \frac{\Delta P_c^{rev}\,(S = 1)\,\phi}{\gamma_{lv} S' \rho (1 - \phi)} \qquad [5]$$

where θ is the contact angle, ΔP_c^{rev} $(S = 1)$ is the capillary pressure, ϕ is the preform porosity, γ_{lv} is the liquid-vapor surface tension, S' is the surface area per unit mass of powder, and ρ is the powder density. This equation allows conversion between the capillary pressure and the contact angle.

In general, the filling process will be neither complete nor reversible, and the relationship between the capillary pressure and the contact angle will depend upon quantities that are not easily determined, such as the extent of irreversibility and the changes in liquid-vapor and solid-vapor surface area. However, if the ratio R of the experimentally measured capillary pressure, $\Delta P_c^{expt}(S_u)$, to the capillary pressure for complete and reversible infiltration, ΔP_c^{rev} $(S = 1)$, can be estimated, then the contact angle can be estimated as follows:

$$\cos\theta = \frac{-1}{R}\left(\frac{\Delta P_c^{expt}(S_u)\phi}{\gamma_{lv} S' \rho (1 - \phi)}\right) \qquad [6]$$

Generally, the ratio $R = \Delta P_c^{expt}(S_u)/\Delta P_c^{rev}$ $(S = 1)$ is expected to be greater than one. In Eq. [6], $\cos\theta$ will decrease as the ratio R increases from one. For nonwetting fluids, θ will also decrease as the ratio R increases from one. Therefore, for nonwetting fluids, a maximum value of the contact angle will be obtained if the ratio R is set equal to one.

Although experimental work on porous media consisting of packed nonspherical particles would provide the $\Delta P_c^{expt}(S_u)/\Delta P_c^{rev}$ $(S = 1)$ ratio information most relevant to this work, to our knowledge, no such work has been published that would allow calculation of the ratio over a wide contact angle range. Therefore, the ratio $R = \Delta P_c^{expt}(S_u)/\Delta P_c^{rev}$ $(S = 1)$ was estimated from the experimental work of Yang *et al.*[9] on drainage of organic fluids from siliconized bead packs. Figure 2 shows the ratio R plotted as a function of advancing contact angle through the nonwetting fluid as measured in sessile-drop experiments. In generating this plot from the data in Reference 6, it was necessary to establish a convention for determining $\Delta P_c^{expt}(S_u)$. Since it is unlikely that

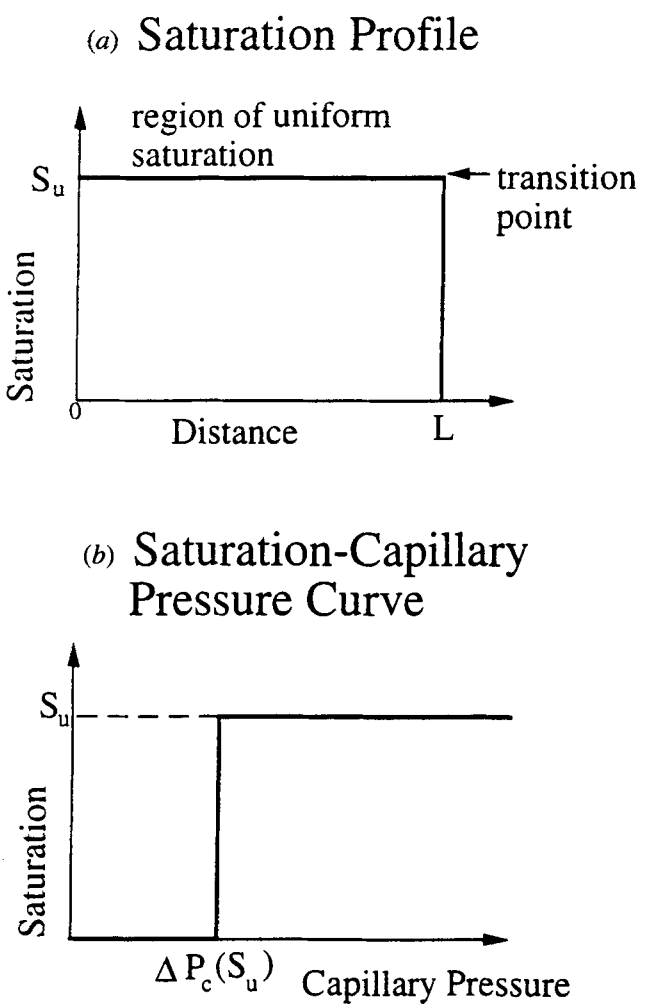

Fig. 1—Idealized saturation profile and saturation *vs* capillary pressure curve. The unsaturated slug flow infiltration model discussed in the text is based upon the idealized saturation profile shown in (*a*). In (a), the saturation is uniform at S_u up to the infiltration front at $x = L$, where it sharply decreases to zero. Such a saturation profile would be consistent with the saturation *vs* capillary pressure curve shown in (*b*), where the saturation rapidly increases from zero to S_u as the capillary pressure increases and then remains at S_u despite further increases in the capillary pressure.

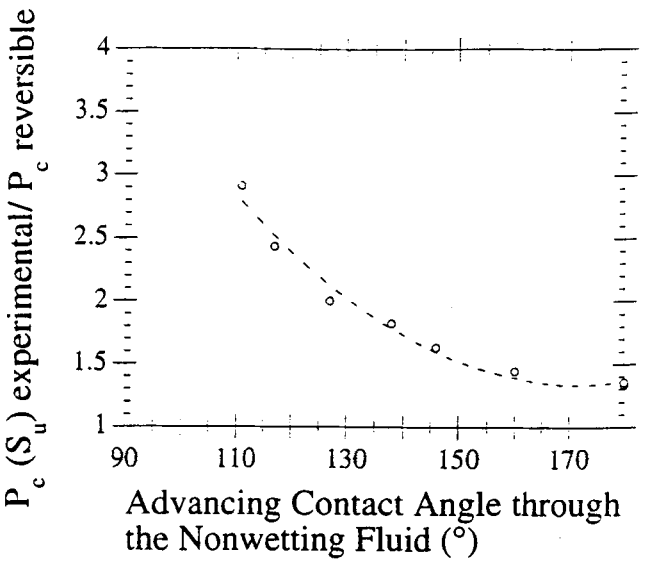

Fig. 2—Ratio of the experimental to the reversible capillary pressure as a function of contact angle. These data have been calculated from the drainage curves in Ref. 9. The dotted curve represents the second-order least-squares fit through the data points: $y = 13.0 - 0.136X + 0.00396x^2$.

saturation differences of less than 5 pct could be determined through examination of solidified polished samples like those obtained in this work, the pressure at which the nonwetting fluid saturation was 5 pct lower than its final value was taken as a practical measure of $\Delta P_c^{expt}(S_u)$. As expected, Figure 2 shows that the ratio R is greater than one. Since Figure 2 indicates that the ratio depends upon the contact angle, which is not known, this method determines a likely contact angle range rather than a precise contact angle value.

III. EXPERIMENTAL MATERIALS AND PROCEDURE

A. *Materials*

The preforms used in these experiments consisted of 99.7 pct pure α-alumina particles whose density was 3.95×10^5 kg/m^3. After sedimentation treatment, over 90 wt pct of the particles ranged between 5 and 15 μm. Brunauer-Emmett-Teller (BET) measurements of the sedimented powder gave an average surface area of 695 m^2/kg. The preforms were packed to an average density of 51 pct in similar purity alumina sample tubes of average i.d. of 4.9 mm and o.d. of 6.3 mm. The average permeability of these preforms was determined as 6.3×10^{-14} m^2 to water and 9.9×10^{-14} m^2 to nitrogen.

Pure Al, an Al 2.3 wt pct Mg alloy, and an Al 5.8 wt pct Mg alloy were used. Limited chemical analysis of the metal in the crucible after the experiment revealed that the final Mg content of the 2.3 wt pct alloy was approximately 1.8 to 1.9 wt pct, while the final Mg content of the 5.8 wt pct alloy was approximately 2.7 wt pct. To reflect the loss of Mg in a simple way, in the rest of this article, the lower Mg content alloy will be referred to as Al-2Mg, while the higher Mg content alloy will be referred to as Al-3Mg. All three metals were tested at 750 °C, while the Al-2Mg alloy was also tested at 850 °C. All experiments were conducted in an argon atmosphere.

B. *Procedure*

Figure 3 illustrates the pressure chamber used to conduct the pressure infiltration experiments and the placement of the sample within the apparatus. The furnace consisted of two sections that were independently controlled. Thermocouples measured the temperature at two points along the sample assembly, as indicated by the x's. For simplicity, the thermal insulation and chill rod assembly inside the sample tube above the preform are not shown in Figure 3. Also omitted are the details of the pressurization, venting, and evacuation lines connected to the pressure chamber and sample tube. Pressure transducers were attached to the base of the pressure

chamber and to the sample tube line at the lid of the chamber.

Before the infiltration portion of the experiment, the chamber and the sample tube were evacuated and backfilled with argon gas. The infiltration portion of the experiment consisted of a pressurization step followed by a venting step. First, both the sample tube and the pressure chamber were pressurized with gas. The furnace controls were adjusted until both the upper and lower indicated temperatures were within the desired temperature range and fairly stable. The temperature range was ±10 °C of the nominal experiment temperature for the Al experiments and ±5 °C for the others. Infiltration of the preform was started by venting the gas in the sample tube to the atmospheric pressure reservoir. Re-equalization of pressure between the sample tube and the pressure chamber halted the infiltration. The creation of a pressure difference between the pressure chamber and the sample tube by venting gas from the sample was an unusual procedure but was necessary to minimize variations in sample temperature during the experiment. Changes in sample temperature could have affected the infiltration distance measurement technique.

The infiltration distance was indicated by the capacitance between the liquid metal inside the sample tube and a cylindrical electrode placed on the outside of the tube. The details of the capacitance technique have been described previously,[10,11] so they will be discussed here only briefly.

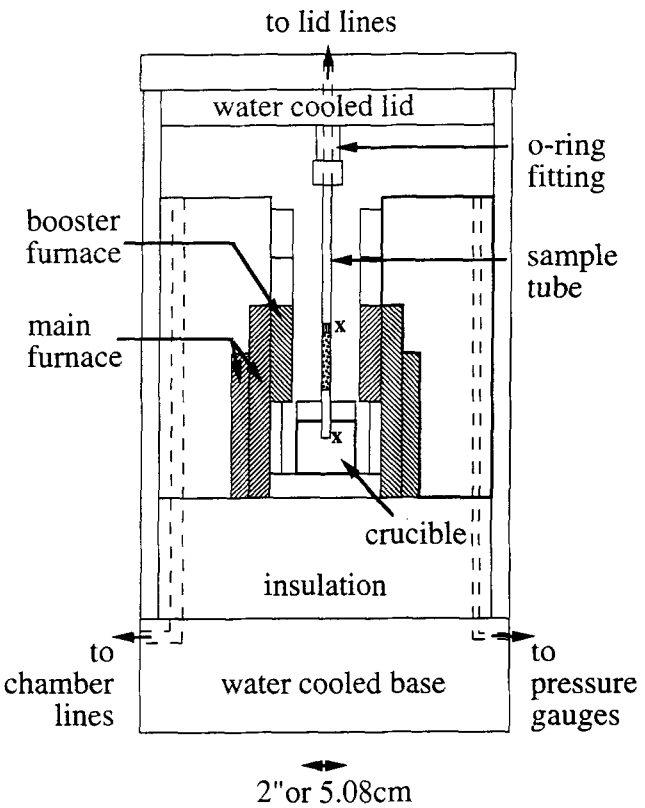

Fig. 3—Schematic of the pressure infiltration unit. This figure illustrates the relative dimensions of the various parts of the unit described in the text. The dotted region of the tube indicates the location of the powder preform. The heavy lines in the crucible interior indicate liquid metal.

The electrode geometry ensured that the capacitance was proportional to the infiltration distance. Since the capacitance-measuring circuit provided a voltage output proportional to capacitance, the circuit output was proportional to infiltration distance. Because of variations in the proportionality between circuit voltage and infiltration distance from one experiment to another, the proportionality constant was determined for each experiment.

IV. RESULTS AND DISCUSSION

A. *Capacitance Circuit Signal during the Infiltration Experiments*

Figure 4 illustrates a typical capacitance circuit signal recording for an experiment with a low initial signal level. For experiments with both low and high initial signal levels, from 1 to 2 seconds after the sample line pressure began to decrease, a plateau region of approximately constant circuit signal often appeared. After some time, the plateau region ended, and the circuit signal began to increase. The increase usually occurred after the pressure transducer in the sample line at the lid of the pressure vessel indicated atmospheric pressure and the applied pressure difference became constant. When the signal was replotted as $(V - V_{plateau})^2$ *vs* time after the plateau ended, the slope of this curve at first tended to increase with time after the plateau but eventually became approximately constant. After the experiment was stopped and the pressure in the sample space began to increase, the circuit voltage generally began to level off.

The observed plateau in the signal near the beginning of the experiment was identified as resulting from the liquid metal reaching the start of the preform. The plateau resulted from the liquid metal being stopped at the entrance of the preform until enough gas vented from the preform that the metal could enter. This would occur

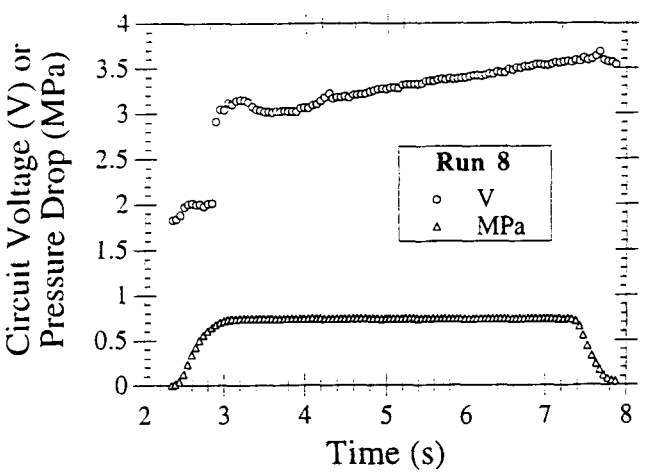

Fig. 4—Typical capacitance circuit signal recording for an experiment with a low initial signal level. The circuit signal is indicated by the circles. The triangle symbol indicates the difference between the pressure in the chamber and the pressure in the sample line at the lid. This pressure difference is not the same as the pressure difference driving the flow, because during venting, the pressure within the preform will tend to be higher than the pressure at the preform exit. However, it is the closest measurable indicator of the pressure difference driving the flow.

when the pressure difference driving the flow, that is, the pressure in the chamber minus the pressure at the preform entrance, was greater than or equal to the minimum capillary pressure for infiltration. Calculations of the pressure at the preform entrance as a function of time showed that the calculated times at which metal could enter the preform were comparable to those observed experimentally.[11]

The increase in signal following the plateau corresponded to infiltration of the preform. Darcy's law predicts that at a constant applied pressure difference, the infiltration distance squared will be proportional to time whether flow is saturated, unsaturated, or a mixture of the two.[5,12,13] Agreement with Darcy's law was observed at longer times, where $\partial(V - V_{plateau})^2/\partial t$ was approximately constant. At shorter times, the observed increases in $\partial(V - V_{plateau})^2/\partial t$ were identified as due to increases in the pressure difference driving the flow as the gas pressure in the preform decreased.

Voltage values were converted to infiltration distances by subtracting the plateau voltage and then multiplying the difference by the conversion factor between infiltration distance and circuit voltage. The conversion factor was obtained by dividing the final infiltration distance by the difference of the circuit voltage at the end of the experiment and the plateau voltage. The infiltration fronts were not completely planar, so the distances measured were the centerline lengths of the composites.

As the applied pressure increases, $\partial(V - V_{plateau})^2/\partial t$ values should also increase. Average $\partial(V - V_{plateau})^2/\partial t$ values most representative of the full applied pressure difference were determined as follows. For a given experiment, the local values of $\partial(V - V_{plateau})^2/\partial t$ at a given time were determined from the slope of a least-squares fit through 10 $\{(V - V_{plateau})^2, t\}$ points, four preceding and five following the point corresponding to the given time. The local $\partial(V - V_{plateau})^2/\partial t$ values were then plotted as a function of time. Since this plot was not a smooth curve, the curve was smoothed and then examined to see where the slope stopped increasing and began to level off. The time at which the slope began to level off was designated as the cutoff time. The average slope value was determined from the slope of a least-squares fit through all points after the cutoff time. If the local slope did not level off by the end of the experiment, the average value was determined from a least-squares fit through points at the end of the experiment. Enough points were selected that the average value did not change much with addition of another point. Further details of the procedure have been given previously.[11]

B. *Capillary Pressures*

The observed relationship between $\partial L^2/\partial t$ and ΔP_{tot} data is consistent with the linear relationship predicted by the unsaturated slug flow infiltration model described in Section II–A. Figure 5 shows the relevant plot for Al along with the least-squares fit line. To two significant figures, the R values from the least-squares fits were 0.81 for Al at 750 °C, 1.0 for Al-2Mg at 750 °C, 0.96 for Al-3Mg at 750 °C, and 0.78 for Al-2Mg at 850 °C. Standard statistical methods[14] were used to determine the uncertainty in the slope and pressure axis intercept for each line.

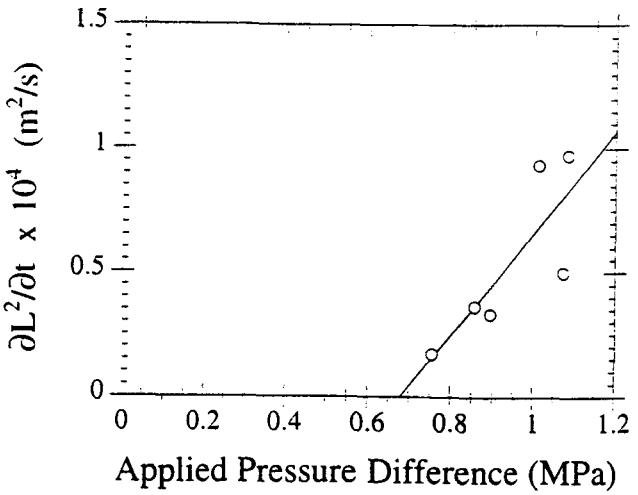

Fig. 5—Linear relationship between $\partial L^2/\partial t$ and ΔP_{tot} obtained for Al at 705 ± 10 °C. This figure shows a typical plot of $\partial L^2/\partial t$ and ΔP_{tot}. Although some scatter was present in the data, the data are consistent with the linear relationship predicted by the unsaturated slug flow model.

Table I displays the pressure axis intercepts. Figure 6 allows visual comparison of the ranges spanned by the 70 pct confidence interval for the pressure axis intercepts. The overlapping of the confidence intervals indicates that the difference in the values was not significant.

Table I. Slopes and Intercepts Calculated for the Experiments

Run Conditions	Slope (m^2/sPa)	Slope Error (m^2/sPa)	Intercept (MPa)
Al, 750 °C	2.1×10^{-10}	7×10^{-11}	0.68
Al-2Mg, 750 °C	2.7×10^{-10}	1×10^{-11}	0.63
Al-3Mg, 750 °C	1.8×10^{-10}	3×10^{-11}	0.59
Al-3Mg, 850 °C	2.8×10^{-10}	1.3×10^{-10}	0.59

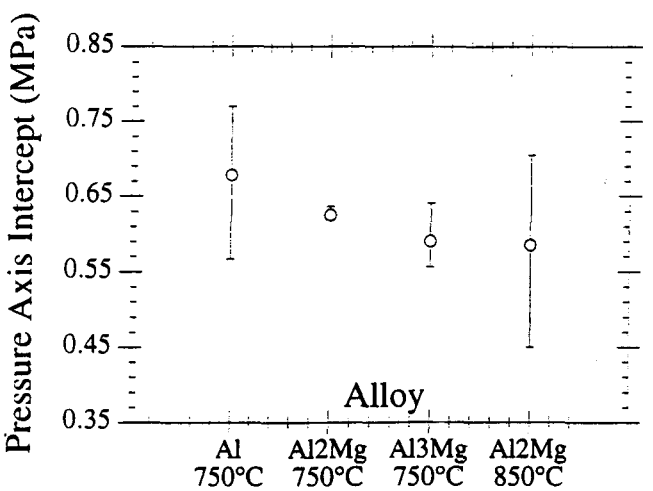

Fig. 6—Comparison of the pressure axis intercepts for the different alloys. The error bars indicate 70 pct confidence intervals for each value. The overlapping of the confidence intervals shows that the difference in the values is not significant.

Table I also displays the calculated slope values. The infiltration model predicts the slope of the line relating $\partial L^2/\partial t$ and ΔP_{tot} will be equal to $2k(S_u)/\mu S_u \phi$. Although S_u and $k(S_u)$ were not known, comparison of the experimentally observed values with the calculated values for saturated flow allows assessment of whether reasonable experimental values were obtained. The slope value for saturated flow was calculated as 2.5×10^{-10} $m^2s^{-1}Pa^{-1}$ at 750 °C and 2.9×10^{-10} $m^2s^{-1}Pa^{-1}$ at 850 °C. Aluminum viscosity data were used in the calculation[15] since experimental results show the viscosity of low Mg content alloys is of little difference.[16] The experimental values are lower than the saturated slope values, except for A1-2Mg at 750 °C. However, when the 2σ error bars for the experimental values are considered, the experimental and calculated values overlap, except for Al-3Mg, which remains slightly below the calculated value. Therefore, the experimentally observed values are at least of the right order of magnitude. Agreement between the experimental and the saturated slope values indicates that the term $k(S_u)/S_u$ was not far from k_{sat}, the saturated permeability.

C. *Contact Angles*

The thermodynamic energy balance described in Section II–B was used to calculate the predicted contact angles for a reversible process, which are listed in Table II. These values are also estimates of the maximum contact angle θ_{max}. To estimate the contact angles for an irreversible process, correction factors were estimated using the maximum contact angle values and the least-squares fit curve in Figure 2. Table II lists the predicted irreversible contact angles and correction factors. A value for Al-2Mg at 850 °C was not calculated because experimental data for the surface tension of the alloy near that temperature was not available. The value of the surface tension of aluminum used in the calculations was 0.883 N/m.[15] The surface tension of Al-2Mg was estimated as 0.82 N/m and that of Al-3Mg as 0.80 N/m from the measurements of Garcia-Cordovilla *et al.*[17] at 700 °C.

The small difference in the capillary pressures translated into a negligible difference in the contact angles. Although it is possible that the contact angles for the alloys were different and the correction factors chosen were incorrect, the trend in Figure 2 indicates that any significant difference should have been reflected in P_c.

The values of θ_{max} indicate that the oxide layer on the surface of the liquid metal has been partially disrupted or modified. The contact angle of Al alloys on alumina has been shown to depend strongly on whether an oxide layer is present on the surface of the liquid metal. Laurent *et al.*[18] performed high vacuum experiments wherein the oxide layer was partially removed, permitting true contact between the metal and the ceramic. These investigations found the contact angle of pure aluminum on single-crystal alumina was 99 ± 6 deg at 750 °C, based on the correlation obtained by Laurent *et al.*[18] When the oxide layer prevents contact between the metal and the ceramic, much higher contact angles are typically observed, ranging from 125 to 155 deg at 750 °C.[1,2,19] The 106 deg maximum contact angle obtained for pure Al in this study is closer to the values obtained by Laurent *et al.* than to those where the oxide layer was present. Since our test atmosphere was not as clean as that of Laurent *et al.*, it is likely that breakage or partial removal of the oxide layer occurred as the liquid metal flowed through the preform. Similarly, low contact angles have been found for infiltration of SAFFIL* alumina fiber preforms with pure aluminum at lower temperatures, and a similar explanation has been proposed.[8] In contrast, Alonso *et al.*[20] concluded that an oxide layer was present on the surface of the liquid metal during their pressure infiltration experiments. However, in their experiments, no attempt was made to evacuate and backfill the preforms. In addition, their modified Eq. [11] for smaller particle sizes predicts a threshold pressure over 1.6 MPa for the 0.51 pct dense 10-μm particle preforms used in this work. This pressure is much higher than the $\Delta P_c(S_u)$ values observed in this work.

*SAFFIL is a trademark of ICI Americas, Inc., Wilmington, DC.

Our observation that Mg additions had little effect on wettability contrasts with studies that have found that such additions markedly improve wetting. Weirauch states that he saw evidence of reactive wetting in sessile-drop experiments in the Al-6Mg/Al_2O_3 system,[1,2] although he was not able to measure contact angles on these particular sessile drops. In the LANXIDE process, spontaneous infiltration of alumina particulates with Al-Mg alloys in a nitrogen atmosphere has been observed.[4] However, since the reaction product formed was AlN, the results are not applicable to our experiments.

In oxygen-containing atmospheres, the improved wetting is commonly attributed to formation of $MgAl_2O_4$ spinel, with the negative free energy of the reaction driving wetting. In these studies, the magnesium alloys did react with the alumina particulates; reaction product was found up to the infiltration front. Thermodynamic calculations[21,22] have shown that both MgO and Al_2MgO_4 have a negative free energy of formation and so are possible reaction products. Experimental evidence exists for the formation of both phases in the magnesium range of interest in these experiments.[1–3,21] The reaction product found in these experiments was not definitively identified but is assumed to be MgO, Al_2MgO_4, or some mixture of the two, as found in the previous experimental work. Whatever the reaction product, the reaction seems to have had little effect since the contact angle of the Mg-containing alloys was only slightly less than that of pure Al.

Table II. Contact Angles Calculated from the Experiments

Run Conditions	θ Reversible (θ_{max})	Estimated $\Delta P_c^{expt}(S_u)/\Delta P_c^{rev}$ ($S = 1$)	θ Irreversible
Al, 750 °C	106 deg	3.1	95 deg
Al-2Mg, 750 °C	105 deg	3.0	95 deg
Al-3Mg, 750 °C	105 deg	3.0	95 deg

However, reaction may not always cause reactive wetting. For example, experiments have shown that no reactive wetting takes place when the reaction occurs ahead of the three-phase contact line.[23] It might also be imagined that with a moving contact line, such as in our experiments, much of the reaction will occur behind the contact line if the reaction kinetics are too slow.

If reactive wetting did not occur because the reaction kinetics were too slow, Mg would primarily affect the contact angle through adsorption at the solid-liquid and liquid-vapor interfaces. To estimate the effect of adsorption, the calculation method developed by Li *et al.*[24] can be used. The calculations predict that Mg would decrease the contact angle, but only by 2 deg at 800 °C.[11] This 2 deg decrease is a rough estimate, since the calculation method can produce results that only qualitatively agree with experimental results.

Alloying with magnesium has been found to modify the oxide layer on the surface of the liquid metal.[1,2,25] In particular, Weirauch[1,2] found that the contact angle for Al-3Mg on alumina was 93 deg after 1000 minutes at 800 °C while that for pure Al was 114 deg. Magnesium loss occurred from the alloy during the sessile-drop experiment. Weirauch interpreted the lower contact angle as resulting from the oxide layer on the sessile drop becoming nonprotective. The 93 deg contact angle value is quite close to the estimated contact angle of 95 deg at 750 °C for Al and the Al-Mg alloys in this work. However, since the wetting results for Al indicate that some removal of the oxide layer did occur, magnesium may have had little additional effect. Therefore, the small influence of Mg on the wetting in these experiments can be explained by the following: absence of reactive wetting at the infiltration speeds present in the experiments, partial disruption of the oxide layer on the surface of the liquid metal during the infiltration process, and potentially small adsorption effects.

V. SUMMARY

Analysis of infiltration data using an unsaturated slug flow model gave characteristic capillary pressures that were not significantly different for Al at 750 °C, Al-2Mg at 750 °C and 850 °C, and Al-3Mg at 750 °C. Therefore, Mg additions are not expected to significantly ease the pressure infiltration process in atmospheres with significant amounts of oxygen. Maximum contact angles calculated from the characteristic capillary pressures using a thermodynamic energy balance were 106 deg for Al and 105 deg for Al-2Mg and Al-3Mg, all at 750 °C. The contact angle obtained for Al indicates partial removal of the oxide layer on the surface of the liquid metal during the infiltration process. The only slightly lower contact angle found for the Mg alloys indicates that Mg concentrations of approximately 2 to 3 wt pct did little to improve the wetting, even though reaction product was formed at the matrix-particle interface. The small effect of Mg on the wetting may be due to absence of reactive wetting at the infiltration speeds present in the experiments and to partial disruption of the oxide layer on the surface of the liquid metal during the infiltration process.

ACKNOWLEDGMENTS

This work was funded by IST/SDI-ONR under Contract No. N00014-90-J-1812. Additional support was provided by the Consortium for the Processing and Evaluation of Inorganic Composites and by the Office of Naval Research under Grant No. N00014-93-11213. Norton Co. donated the ceramic powder. The authors would also like to thank Professors A. Mortensen, MIT, and N. Eustathopoulos, Institut National Polytechnique de Grenoble, for suggestions offered during discussions of the work.

REFERENCES

1. D.A. Weirauch: *J. Phys. (Paris)*, 1988, vol. 49, pp. C5:387-C5:394.
2. D.A. Weirauch: *J. Mater. Res.*, 1988, vol. 3, pp. 729-39.
3. B.C. Pai and R. Subrat: *Mater. Sci. Eng.*, 1976, vol. 24, pp. 31-44.
4. M.K. Aghajanian, M.A. Rocazella, J.T. Burke, and S.D. Keck: *J. Mater. Sci.*, 1991, vol. 26, pp. 447-54.
5. D. Hillel: *Soil and Water: Physical Principles and Processes*, Academic Press, New York, NY, 1971, p. 114.
6. L.R. White: *J. Colloid Interface Sci.*, 1982, vol. 90, pp. 536-38.
7. S.-Y. Oh, J.A. Cornie, and K.C. Russell: *Metall. Trans. A*, 1989, vol. 20A, pp. 527-32.
8. A. Mortensen and T. Wong: *Metall. Trans. A*, 1990, vol. 21A, pp. 2257-63.
9. Y.-W. Yang, G. Zografi, and E.E. Miller: *J. Colloid Interface Sci.*, 1988, vol. 122, pp. 24-34.
10. T.R. Fletcher, J.A. Cornie, and K.C. Russell: *Mater. Sci. Eng.*, 1991, vol. A144, pp. 159-63.
11. T.R. Jonas: Ph.D. Thesis, Massachusetts Institute of Technology, Cambridge, MA, 1993.
12. A. Mortensen, L.J. Masur, J.A. Cornie, and M.C. Flemings: *Metall. Trans. A*, 1989, vol. 20A, pp. 2535-47.
13. J.R. Philip: *Soil Sci.*, 1958, vol. 85, pp. 278-86.
14. N.R. Draper and H. Smith: *Applied Regression Analysis*, Wiley, New York, NY, 1966, pp. 18-21.
15. *Smithells Metals Reference Book*, C.A. Brandes, ed., Butterworth and Co., Boston, MA, 1983, p. 7.
16. E. Gebhardt, M. Becker, and S. Dorner: *Aluminium (Dusseldorf)*, 1955, vol. 31, pp. 315-21.
17. C. Garcia-Cordovilla, E. Louis, and A. Pamies: *J. Mater. Sci.*, 1986, vol. 21, pp. 2787-92.
18. V. Laurent, D. Chatain, C. Chatillon, and N. Eustathopoulos: *Acta Metall.*, 1988, vol. 36, pp. 1797-1803.
19. J.J. Brennan and J.A. Pask: *J. Am. Ceram. Soc.*, 1968, vol. 51, pp. 569-73.
20. A. Alonso, A. Pamies, J. Narciso, C. García-Cordovilla, and E. Louis: *Metall. Trans. A*, 1993, vol. 24A, pp. 1423-32.
21. C.G. Levi, G.J. Abbaschian, and R. Mehrabian: *Metall. Trans. A*, 1978, vol. 9A, pp. 697-711.
22. A.D. McLeod: in *Fabrication of Pariticulates Reinforced Metal Composites*, J. Masounave and F.G. Hamel, eds., ASM INTERNATIONAL, Materials Park, OH, 1991, pp. 17-21.
23. V. Laurent, D. Chatain, and N. Eustathopoulos: *Mater. Sci. Eng.*, 1991, vol. 135A, pp. 89-94.
24. J.G. Li, L. Coudurier, and N. Eustathopoulos: *J. Mater. Sci.*, 1989, vol. 24, pp. 1109-16.
25. A. Mortensen and I. Jin: *Int. Mater. Rev.*, 1992, vol. 37, pp. 101-28.